Appl. Phys. B (2015) 119:313–318
DOI 10.1007/s00340-015-6066-4

Applied Physics B
Lasers and Optics

3D measurements of ignition processes at 20 kHz in a supersonic combustor

Lin Ma · Qingchun Lei · Yue Wu · Timothy M. Ombrello · Campbell D. Carter

Received: 5 February 2015 / Accepted: 20 February 2015 / Published online: 5 March 2015
© Springer-Verlag Berlin Heidelberg 2015

Abstract The ignition dynamics in a Mach 2 combustor were investigated using a three-dimensional (3D) diagnostic with 20 kHz temporal resolution. The diagnostic was based on a combination of tomographic chemiluminescence and fiber-based endoscopes (FBEs). Customized FBEs were employed to capture line-of-sight integrated chemiluminescence images (termed projections) of the combustor from eight different orientations simultaneously at 20 kHz. The measured projections were then used in a tomographic algorithm to obtain 3D reconstruction of the sparks, ignition kernel, and stable flame. Processing the reconstructions frame by frame resulted in 4D measurements. Key properties were then extracted to quantify the ignition processes, including 3D volume, surface area, sphericity, and velocity of the ignition kernel. The data collected in this work revealed detailed spatiotemporal dynamics of the ignition kernel, which are not obtainable with planar diagnostics, such as its growth, movement, and development into "stable" combustion. This work also illustrates the potential for obtaining quantitative 3D measurements using tomographic techniques and the practical utility of FBEs.

L. Ma (✉) · Y. Wu
Department of Aerospace and Ocean Engineering, Virginia Tech, Blacksburg, VA 24060, USA
e-mail: linma@vt.edu

L. Ma · Q. Lei
Department of Mechanical Engineering, Virginia Tech, Blacksburg, VA 24060, USA

T. M. Ombrello · C. D. Carter
Air Force Research Laboratory, Dayton, OH 45433, USA

1 Introduction

Reliable ignition in high-speed flows represents a significant scientific problem with a wide range of practical applications. Scientifically, the ignition processes involve complicated interactions among various aspects of chemical reaction and turbulence, which are not fully understood yet [1]. Reliable ignition in propulsion and power devices is further complicated by practical factors such as the relatively long chemical timescales of practical hydrocarbon fuels and the nonideal geometry of practical devices [1, 2]. As a result, a significant amount of research has been invested for a better understanding of the ignition processes at a fundamental level and also for the design of practical devices [1–3]. This work reports an experimental study of the ignition processes in supersonic (Mach 2) flows. Non-intrusive techniques are usually desired or required for experimental study in supersonic flows, and a range of optical diagnostics has been employed in past efforts ranging from chemiluminescence [4] and schlieren [3] imaging to planar laser-induced fluorescence (PLIF) [5, 6] and particle image velocimetry (PIV) [2]. Results from these past efforts all reveal highly transient and 3D flow and flame structures during the ignition processes, but the diagnostics employed are not capable of fully resolving transient, 3D events. Therefore, there is a need for measurements that can resolve the ignition processes with the required temporal resolution, spatial resolution, and also dimensionality.

Based on the above understanding, this work reports 3D measurements of the ignition processes in a supersonic combustor at 20 kHz. The measurements were made in the Research Cell 19 supersonic wind tunnel facility housed at the Air Force Research Laboratory (AFRL) [7]. The measurements were obtained using a combination of tomographic chemiluminescence (TC) and fiber-based

endoscopes (FBEs), an approach recently developed and demonstrated in both laboratory and practical flames [8–10]. The TC technique relies on capturing line-of-sight integrated chemiluminescence images simultaneous from various orientations, which are then used as inputs in a tomographic algorithm to obtain 3D reconstructions [11–13]. The use of FBEs has been demonstrated to significantly facilitate the implementation of the TC technique [8–10]. In the current work, the TC technique enabled measurements of the 3D shape, volume, surface area, and velocity of the ignition kernels in a Mach 2 cavity-based flameholder.

2 Experimental setup

The experimental setup is illustrated schematically in Fig. 1. The experiments were performed in a supersonic wind tunnel housed in Research Cell 19 at AFRL as detailed previously [2, 4]. The facility is capable of operating continuously with peak stagnation conditions of 2860 kPa and 922 K at flow rates up to 15 kg/s [7, 14]. Figure 1a illustrates the overall experimental setup from the end view (where the fuel flow issues out of the page), and Fig. 1b shows a side view (with air flow from left to right) of the generic cavity configuration used in this work. The entire flow path is 152 mm wide, and there are two ports in the base of the cavity located 19 mm on either side of the symmetry plane to accommodate spark plugs [2]. The two spark plugs (represented by the star symbols) were fired simultaneously, each with a delivered energy of approximately 100 mJ/pulse, to ignite the mixture within the cavity. Fuel (C_2H_4) was injected into the cavity from eleven holes in the cavity closeout ramp as shown. A flow Mach number of 2, a total temperature of approximately 610 K, and a total pressure of approximately 483 kPa were used for all experiments. There was optical access from both the sides and the top through fused silica windows, allowing for examination of the cavity ignition and burning process from multiple views as used in this work and as shown in Fig. 1a.

Chemiluminescence was captured from eight orientations simultaneously (see Fig. 1a), using eight FBE inputs and two CMOS (complimentary metal-oxide semiconductor) cameras (Photron SA-Z). The FBEs used here were customized and described in detail in [10, 15, 16]. These FBEs were provided as two customized bundles, with four inputs in each bundle. The four inputs in each bundle are then combined into one output, so that chemiluminescence images captured by all four inputs can be acquired by one camera. More specifically, as Fig. 1a schematically shows, camera 1 captured the chemiluminescence images from FBE inputs 1–4 of bundle 1, and camera

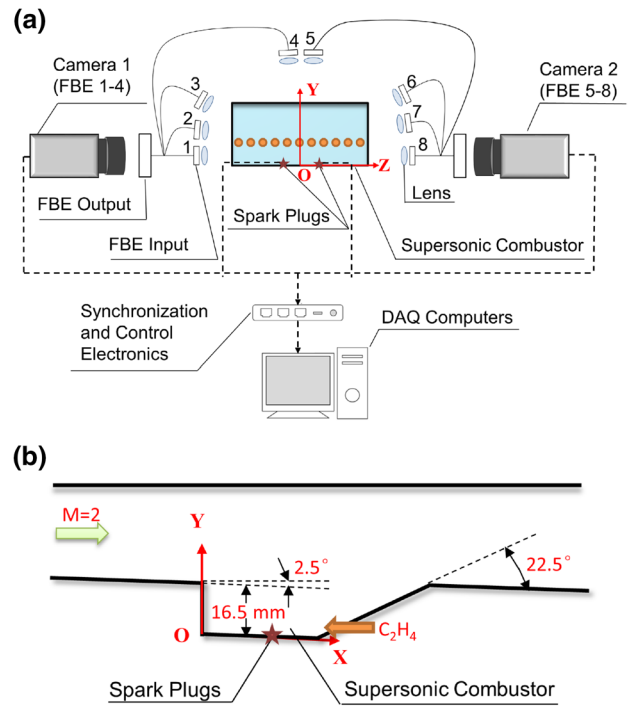

Fig. 1 Experimental setup. **a** The overall experimental setup and end view of the wind tunnel (the fuel flow issues out of the page). **b** The wind tunnel from the side view

2 the images from FBE inputs 5–8 of bundle 2. A lens (105 mm focal length and f/2.8) was placed in front of each FBE input to enlarge the collection angle. Each FBE input consists of an array of 470 × 470 (220,900) individual single-mode fibers, and therefore, the output of each bundle transmits a total of 883,600 (4 × 220,900) image elements to the camera, which operated at a pixel resolution of 1024 × 1024. The FBE bundles and cameras were aligned in such a way that one image element transmitted by the FBE approximately corresponded to one pixel on the camera. This arrangement provided a good and reasonable match with regard to spatial resolution between available FBEs and cameras. One of the FBE bundles had an overall length of 1.35 m and the other 2 m. The FBE bundles are flexible and have a smaller footprint than the camera, greatly facilitating the experimental setup in the supersonic wind tunnel facility. The FBEs have no transmission for wavelengths below 400 nm or above 1.2 μm, and thus, the FBE acts as a wide bandpass filter. In the visible range used in this work, the FBE bundles cause an attenuation of 7–10× [16]. Tests have been performed with a narrow bandpass filter (centered at 430 nm, where CH* emission peaks, with a 10 nm FWHM), and the signal was not sufficiently high with the cameras available to this work. Thus, the chemiluminescence measurements used here were obtained without any additional filtering,

and the signal primarily consisted of contributions from CH* and C_2* in the visible range (as confirmed by emission spectra employing a spectrometer).

The cameras were operated at a frame rate of 20 kHz and an exposure time of approximately 50 µs. The pixel resolution of the cameras decreases as the frame rate increases beyond 20 kHz. Therefore, with these cameras, there is a tradeoff between temporal and spatial resolution above 20 kHz. Before the ignition measurements were conducted, a calibration target was placed in the tunnel to determine the orientation and location of the FBEs using a view registration program [10]. All eight FBE inputs were aligned in the plane perpendicular to the flow (i.e., the *YZ* plane as shown), and their orientations (defined as the angle formed relative to the *Z* axis) were 180°, 169°, 144°, 92°, 89°, 38°, 18°, and 0°, respectively, for FBE inputs 1 through 8. The arrangement of the FBEs was a result of both scientific considerations (to obtain the greatest number of independent projections on each FBE) and practical constraints (primarily optical access and availability of physical space). For example, placement of the FBEs at 89° and 92° was dictated by practical constraints, though note that even redundant measurements (e.g., two measurements at the exact same orientation) can help to reduce reconstruction uncertainty.

Control electronics were used to synchronize the operation of the cameras and spark plugs as shown in Fig. 1a. Measurements were performed under a range of fuel flow rates, and chemiluminescence images were captured for a duration of 0.05 s for each run (resulting in a total of 1000 frames per FBE input) to cover the entire process of ignition and transition into stable combustion (if the run resulted in stable combustion). This work, however, mainly focuses on the ignition portion of the measurements.

The synchronization scheme and the nature of the measurements are best explained with the aid of Fig. 2, which shows two frames of chemiluminescence images captured by camera 2. The cameras began framing at the same time that the spark plugs began to charge. Sparks were initiated about 9 ms after charging began. Time zero ($t = 0$) is defined as the time that a spark first appears. The sparks lasted for 3–4 ms, during which time the ignition kernel(s) developed and transitioned into stable flames under certain operating conditions (i.e., fuel/air ratio). Figure 2a shows the 72nd frame captured by camera 2 (i.e., $t = 3.6$ ms), illustrating the co-existence of the sparks and the resulting ignition kernel. As noted, camera 2 captured the images transmitted by FBE inputs five through eight (as labeled here), and the image transmitted by each FBE inputs occupied a quarter of the camera chip (i.e., ~512 × 512 pixels). Note that Fig. 2a only shows a cropped region of ~320 × 320 pixels to better display the data. The top left portion of Fig. 2a shows the image captured by FBE input 5 (at an orientation of 89°), showing the two sparks from the top view. The bottom right portion shows the image captured by FBE input eight (at an orientation of 0°), illustrating the overlapping of the sparks from the side view and the ignition kernel. Note that the ignition kernel was not captured by FBE input 5, because the top window offered a smaller field of view (FOV) than the side windows. The chemiluminescence emissions from the ignition kernel(s) were significantly weaker than the emissions from the sparks in all the tests. Signal in the left of each image was the ignition kernel, which was being shed and carried along in the flow toward the leading edge of the cavity; this kernel resulted in subsequent flame propagation and full cavity burning as shown in Fig. 2b for this run. Figure 2b shows the 280th frame (i.e., $t = 14$ ms), captured after the sparks had terminated and a stable flame had developed.

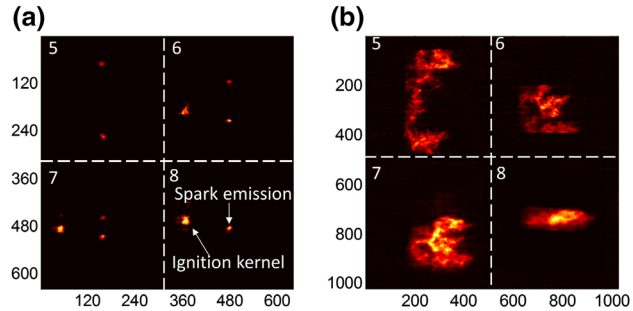

Fig. 2 Two frames of sample projections recorded by camera 2: **a** frame 72 corresponding $t = 3.6$ ms; **b** frame 280 corresponding $t = 14$ ms

3 Results

The line-of-sight integrated chemiluminescence images (termed *projections*) captured by all eight FBEs were used as inputs to a tomographic reconstruction program to obtain the 3D distributions of the chemiluminescence emissions, which were then used to represent the structures of the sparks, ignition kernel(s), and stable flames. Performing the reconstruction frame by frame resulted in a series of 3D measurements resolving the temporal dynamics of the ignition and combustion processes. Figure 3 shows two such 3D reconstructions using the 72nd and 280th frame of the measured projections as inputs (four of the projections captured by camera 2 are shown in Fig. 2). This reconstruction considered a cubical measurement volume with a side length of 64 mm, determined by the FOV captured by all eight FBEs to best encompass the region of interest in the cavity. The measurement volume was then discretized into 128 × 128 × 128 (~2 × 10^6) voxels, resulting

in a dimension of 0.5 mm for each voxel. Such a resolution is not sufficient to resolve all of the fine-scale turbulent features. However, the spatial resolution of tomographic imaging can be improved simply by obtaining more projections from additional orientations. The tomographic algorithm used here was a modified variation of the algebraic reconstruction technique (ART) [12, 17, 18]. The image analyses were performed by a combination of geometrical ray-tracing [17, 19] and Monte Carlo simulation [20, 21], and the approach used here has been validated via numerical simulations [11, 17] and controlled experiments in both nonreactive [15] and reactive flows [11, 17]. Tomographic reconstruction, which at this scale is computationally and memory intensive [18, 22], was performed on a workstation with two Intel Xeon E5 processors and 512 GB of RAM. Processing one frame of the tomographic reconstruction (such as the one shown in Fig. 3a) required approximately 30 min on this workstation.

Figure 3a, d shows the rendering of the 3D reconstruction obtained from the reconstruction. The rendering shown here was based on an iso-surface of the ignition kernel or the flame determined by a thresholding method. More specifically, the iso-surface was determined in three steps. First, the 3D reconstruction was performed. Second, the background noise level was determined from the raw projection measurements. Third, the background noise level was then applied to threshold the 3D reconstruction obtained in step 1 into two zones, those with chemiluminescence signal either higher or lower than the background noise. The two zones were then considered as the no-flame and flame zones, respectively. Figure 3a, d shows the iso-surface separating these two zones. Other methods can be applied to extract the flame front from chemiluminescence images. The method used here was designed to extract the outer edge of the flame to facilitate comparison with 2D line-of-sight averaged chemiluminescence measurements. To aid the interpretation of the 3D reconstructions, Fig. 3b, c, e, and f shows the corresponding projection measurements from the top view (captured by FBE input 5 at 89°) and side view (captured by FBE input eight at 0°). Comparison between the 3D reconstructions and the projection measurements illustrates the validity and utility of the 3D measurements. For example, projection measurement shown in Fig. 3c from the side view cannot reveal the size and irregular shape of the ignition kernel as shown in Fig. 3a. The projection measurement shown in Fig. 3e from the top view suggested (1) a periodic structure in the stable flame along the Z direction and (2) a larger flame near the walls of the tunnel, both of which were fully revealed by the 3D reconstruction shown in Fig. 3d. Based on the reconstructions such as those shown in Fig. 3a, d, 3D properties of the sparks, ignition kernel(s), and flames were extracted, including their size, shape, and location.

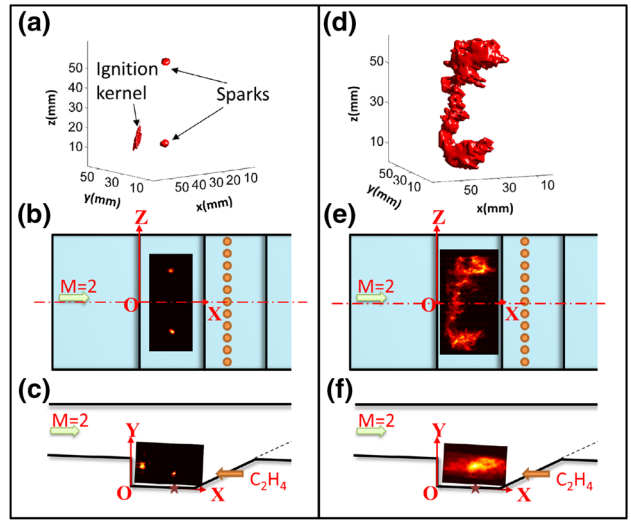

Fig. 3 Comparison of 3D reconstruction with projections measured from the top and side for both the ignition phase (**a**–**c**) and the stable combustion phase (**d**–**f**)

Figure 4 shows the volume of the sparks (or more precisely, the plasmas formed by the sparks) and the ignition kernel for a duration of ~ 4 ms for one experiment, covering the time span from the initiation of the sparks to the transition to a stable flame. In this experiment, C_2H_4 fuel was injected at a flow rate of 95 SLPM (standard liters per minute) into the cavity, representing a fuel-rich operation condition of the flame holder. As can be seen from Fig. 4, the sparks appeared at $t = 0$ and the volumes of the sparks were determined to fluctuate in a relatively narrow range of ~20 to 30 mm^3. The volumes of the two sparks were not equal, with one (spark 2) consistently larger than the other (spark 1). Spark 2 lasted for 3.5 ms and spark 1 for 3.8 ms in this experiment, as clearly seen by the sudden drop of their volumes at 3.5 and 3.8 ms. Energy supplied by the sparks generated high temperatures and radicals in the fuel/air mixture, and the radicals accumulated and their emission increased to a point that it could be captured by the tomographic sensor starting at $t = 3.05$ ms. The volume of the ignition kernel (only one ignition kernel was observed in this specific run) when it first appeared at $t = 3.05$ ms was determined to be 42.5 mm^3 (note that the vertical axis of Fig. 4 is broken into two parts with different scales to accommodate both the volume of the sparks and the ignition kernel). Of course, a more sensitive detector is desired, so that the development of the ignition kernel can be resolved from its very beginning. The ignition kernel initially grew gradually and then explosively between 3.85 and 3.95 ms; this sudden explosive growth in the size of the kernel was used to define the transition to a stable flame. Based on the 3D reconstruction, other 3D properties (i.e., surface area and sphericity) can also be calculated and

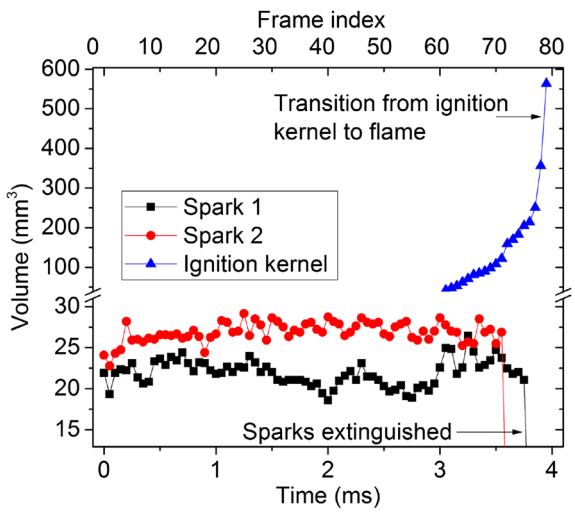

Fig. 4 Volume extracted from the 3D reconstructions of the ignition kernel and the sparks

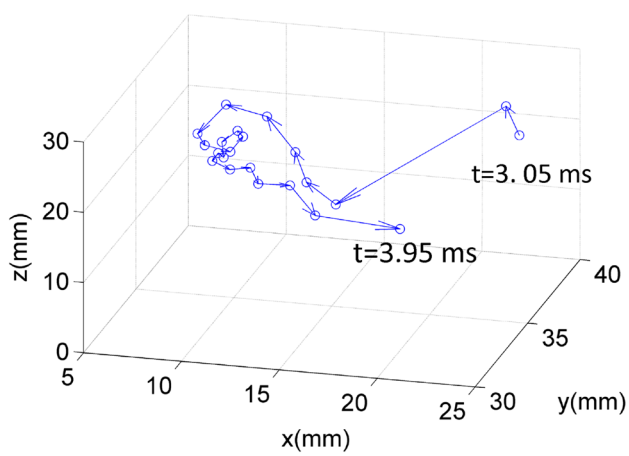

Fig. 5 3D3C velocity vector extracted from the 3D reconstructions of the ignition kernel

statistics obtained, but this work focuses on the development and demonstration of the diagnostics, and elaborated discussion of the results will be reported separately.

Once the 3D shape and location of the ignition kernel were determined, the 3D and three-component (3D3C) velocity of the kernel movement can be calculated as shown in Fig. 5. The velocity vectors shown here were determined by (1) calculating the 3D spatial movement of the centroid of the ignition kernel from frame to frame and (2) dividing the 3D spatial movement by the interval between frames (i.e., 50 µs). The centroid of the ignition kernel was used here to define the spatial movement due to its irregular shape as discussed above, thus introducing uncertainty in the definition of the velocity vector (especially when coupled with chemiluminescence detection limits). However, such uncertainty was

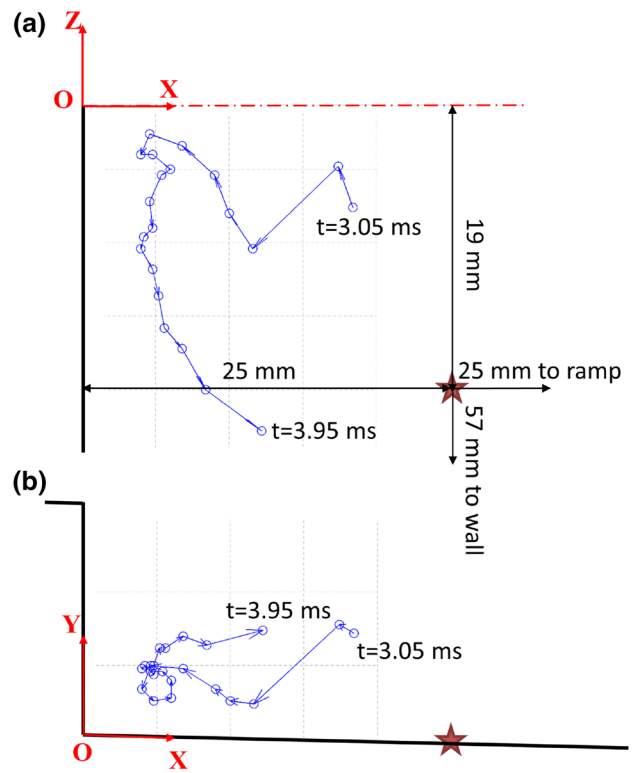

Fig. 6 2D projection of the 3D3C velocity vector from the *top view* (**a**) and the *side view* (**b**)

alleviated by the relatively small kernel volume. Figure 5 shows that the kernel moved in a range of ~20 mm in the *X* direction, ~10 mm in the *Y* direction, and ~30 mm in the *Z* direction before it transitioned into a stable flame. Figure 6 shows the 2D projection of the 3D3C velocity vectors from the top and side view in panel (a) and (b), respectively. Note that to better display the data, (1) Fig. 6a only shows a portion (approximately 25 mm in the *X* direction and 19 mm in the negative *Z* direction) of the cavity in which the kernel had travelled, and (2) the length of the velocity vector is proportional to the spatial movement and is plotted in scale with the dimension of the cavity. The velocity magnitude was determined to be in the range from 20 to 200 m/s, and Fig. 6 shows the trajectory of the kernel in the flowfield. The kernel travelled upstream following the recirculating flowfield formed by the cavity until reaching about 4 mm from the step of the cavity, where it then turned back, travelled downstream, and developed into stable flame propagation. These 3D3C properties extracted here (including the magnitude and pattern) are in reasonable agreement with previous planar velocity measurements obtained via PIV [2], though quantitative comparison is difficult due to the 2D nature of previous results and the 3D nature of the current results. The results shown here demonstrate the utility of the 3D technique to resolve the 3D3C velocity vectors at 20 kHz temporal resolution.

4 Summary and conclusions

This work investigated the ignition process in a cavity within a Mach 2 wind tunnel using 3D measurements at 20 kHz. The measurements were performed using tomographic chemiluminescence in combination with FBEs. Spark-luminosity and chemiluminescence projections (from the combustion reactions) were simultaneously captured from eight orientations using two customized FBE bundles at 20 kHz. The measured projections were then fed into a tomographic algorithm as inputs to obtain the 3D reconstruction of the sparks, ignition kernel, and also stable combustion. Processing the tomographic reconstructions frame by frame resulted in 4D measurements revealing the spatial structures of the spark, ignition kernel, and flame in all three directions and the temporal dynamics with 20 kHz resolution. Based on such 4D data, key properties were extracted to quantify the ignition processes, including 3D volume, surface area, sphericity, and velocity of the ignition kernel. The 3D results in this work revealed detailed dynamics of the ignition kernel that are not obtainable with planar diagnostics, such as its growth, movement, and development into stable combustion.

Acknowledgments This work was supported by the US Air Force Office of Scientific Research (AFOSR) with Dr. Chiping Li as the technical monitor. Some of the image processing and analysis algorithms used here were developed via support provided by an NSF award (Award CBET 1156564). Lin Ma is also grateful for a US Air Force Summer Faculty Fellowship.

References

1. S.J. Shanbhogue, S. Husain, T. Lieuwen, Lean blowoff of bluff body stabilized flames: scaling and dynamics. Prog. Energy Combust. Sci. **35**, 98–120 (2009)
2. S.G. Tuttle, C.D. Carter, K.-Y. Hsu, Particle image velocimetry in a nonreacting and reacting high-speed cavity. J. Propuls. Power **30**, 576–591 (2014)
3. M.B. Sun, C. Gong, S.P. Zhang, J.H. Liang, W.D. Liu, Z.G. Wang, Spark ignition process in a scramjet combustor fueled by hydrogen and equipped with multi-cavities at Mach 4 flight condition. Exp. Therm. Fluid Sci. **43**, 90–96 (2012)
4. T.M. Ombrello, C.D. Carter, C.-J. Tam, K.-Y. Hsu, Cavity ignition in supersonic flow by spark discharge and pulse detonation. Proc. Combust. Inst. **35**, 2101–2108 (2015)
5. M. Ryan, M. Gruber, C. Carter, T. Mathur, Planar laser-induced fluorescence imaging of OH in a supersonic combustor fueled with ethylene and methane. Proc. Combust. Inst. **32**, 2429–2436 (2009)
6. C.C. Rasmussen, S.K. Dhanuka, J.F. Driscoll, Visualization of flameholding mechanisms in a supersonic combustor using PLIF. Proc. Combust. Inst. **31**, 2505–2512 (2007)
7. M.R. Gruber, A.S. Nejad, New supersonic combustion research facility. J. Propuls. Power **11**, 1080–1083 (1995)
8. M. Kang, Y. Wu, L. Ma, Fiber-based endoscopes for 3D combustion measurements: view registration and spatial resolution. Combust. Flame **16**, 3063–3072 (2014)
9. L. Ma, X. Li, W.G. Lamont, K. Venkatesan, S. Wehe, *3D Flame Measurements at 5 kHz on a Jet Fueled Aviation Combustor*. ASME Turbo Expo 2015 (2014)
10. M. Kang, Q. Lei, L. Ma, Characterization of linearity and uniformity of fiber-based endoscopes for 3D combustion measurements. Appl. Opt. **53**, 5961–5968 (2014)
11. X. Li, L. Ma, Capabilities and limitations of 3D flame measurements based on computed tomography of chemiluminescence. Combust. Flame **162**, 642–651 (2015)
12. J. Floyd, P. Geipel, A.M. Kempf, Computed tomography of chemiluminescence (CTC): instantaneous 3D measurements and phantom studies of a turbulent opposed jet flame. Combust. Flame **158**, 376–391 (2011)
13. X. Li, L. Ma, Volumetric imaging of turbulent reactive flows at kHz based on computed tomography. Opt. Express **22**, 4768–4778 (2014)
14. M.R. Gruber, J.M. Donbar, C.D. Carter, K.Y. Hsu, Mixing and combustion studies using cavity-based flameholders in a supersonic flow. J. Propuls. Power **20**, 769–778 (2004)
15. Q. Lei, Y. Wu, H. Xiao, L. Ma, Analysis of four-dimensional Mie imaging using fiber-based endoscopes. Appl. Opt. **53**, 6389–6398 (2014)
16. M. Kang, X. Li, L. Ma, Calibration of Fiber Bundles for Flow and Combustion Measurements, in *AIAA SciTech 2014, Paper AIAA-2014-0397,* (National Harbor, MD, 2014)
17. W. Cai, X. Li, F. Li, L. Ma, Numerical and experimental validation of a three-dimensional combustion diagnostic based on tomographic chemiluminescence. Opt. Express **21**, 7050–7064 (2013)
18. W. Cai, X. Li, L. Ma, Practical aspects of implementing three-dimensional tomography inversion for volumetric flame imaging. Appl. Opt. **52**, 8106–8116 (2013)
19. W. Cai, L. Ma, Improved Monte Carlo model for multiple scattering calculations. Chin. Opt. Lett. **10**, 012901 (2012)
20. Y. Zhao, X. Li, L. Ma, Multidimensional Monte Carlo model for two-photon laser-induced fluorescence and amplified spontaneous emission. Comput. Phys. Commun. **183**, 1588–1595 (2012)
21. X. Li, L. Ma, Effects of line-narrowing of amplified spontaneous emission analyzed by a Monte Carlo model. J. Quant. Spectrosc. Radiat. Transf. **114**, 157–166 (2012)
22. J. Floyd, A.M. Kempf, Computed tomography of chemiluminescence (CTC): high resolution and instantaneous 3-D measurements of a matrix burner. Proc. Combust. Inst. **33**, 751–758 (2011)